Rock Mechanics and Rock Engineering (2021) 54:5807–5825
https://doi.org/10.1007/s00603-021-02591-z

ORIGINAL PAPER

Experimental Investigation on the Mechanism of Coal and Gas Outburst: Novel Insights on the Formation and Development of Coal Spallation

Yang Lei[1,2,3] · Yuanping Cheng[1,2,3,4] · Ting Ren[4] · Qingyi Tu[1,2,3] · Yixuan Li[1,2,3] · Longyong Shu[5]

Received: 14 October 2020 / Accepted: 22 July 2021 / Published online: 5 August 2021

Abstract

The fragmentation of coal produces abundant coal gases and is presumed to be the defining characteristic of coal and gas outbursts. Knowing the mechanism of these catastrophic hazards is one of the most important breakthroughs in mining geology. In the outburst process, coal spallation represents a unique failure type and typically leaves behind a spallation area (with a series of fracture textures) in the coal seam. Revealing its features and formation mechanism is crucial in accurately interpreting the outburst process. In this study, we conducted a series of outburst experiments with different gases, including CO_2, N_2, and He. We establish that a spallation area can develop spontaneously during CO_2 and N_2 tests, whereas an outburst caused by He tests (even under stressed conditions) does not produce a spallation area. That is, the spallation area cannot be observed in non-absorbable gas outbursts. We, therefore, focus on the role of coal gas in spallation and propose a viable mechanism to explain its formation. During the outburst development stage, the influence of gas ad-/desorption is critical, as it controls the width of the spallation area and the spallation thickness. In contrast, stress is not a necessary condition. Whether a spallation area will be produced is particularly determined by the generation of a sufficient internal pressure gradient. Moreover, because of gas desorption, the total outburst energy can be increased by 1.84–5.30 times; and the mean outburst propagation velocity and the mean frequency of coal spallation ejected can be enhanced by 0.38–8.76% and 1.28–12.07%, respectively. Consequently, the destructiveness of outbursts depends on the contribution of desorbed gas.

Keywords Coal and gas outburst · Coal spallation · Experimental simulation · Gas desorption · Energy analysis

List of Symbols

P_i	Gas pressure in the coal at the exposed surface (MPa)
σ_t	Tensile strength of the coal (MPa)
α	Impact factor of the volume stress on the permeability
p_0	Initial gas pressure (MPa)
φ	Porosity (%)
γ^p, γ^{p*}	Softening parameter
E_0	Elastic energy (J)
E_1,E_2	Energy contributions of the desorbed gas and the free gas (J)
M_E	Intensity of outburst (kg)
v_e	Speed of the ejected coal flow (m/s)
σ_x, σ_y, σ_z	Triaxial loading pressures (MPa)
P_a	Ambient atmospheric pressure (MPa)
k	Coal permeability (m^2)
Θ	Volume stress (MPa)
ξ	Jump coefficient for the coal permeability
μ	Poisson's ratio
k_0	Initial coal permeability (m^2)
E_s	Gas expansion energy (J)
h	Characteristic height dimension of ejected coal, $h = 0.6$ m

✉ Yuanping Cheng
ypcheng@cumt.edu.cn

1 Key Laboratory of Gas and Fire Control for Coal Mines, China University of Mining and Technology, Ministry of Education, Xuzhou 221116, China

2 School of Safety Engineering, China University of Mining and Technology, Xuzhou 221116, Jiangsu, China

3 National Engineering Research Center for Coal and Gas Control, China University of Mining and Technology, Xuzhou 221116, Jiangsu, China

4 School of Civil, Mining and Environmental Engineering, University of Wollongong, Wollongong, NSW 2522, Australia

5 Mine Safety Technology Branch, China Coal Research Institute, Beijing 100013, China

L_E	Equivalent distance of coal ejection (m)
g	Acceleration of gravity, $g = 9.8$ m/s^2
V_L, P_L	Adsorption constants

1 Introduction

Coal and gas outbursts (hereafter referred to as outbursts) are one of the most powerful and destructive hazards in underground mining. An outburst is a violent and unstable release of gas and strain energy that occurs in a coal seam, which is accompanied by a sudden ejection of large amounts of coal (rock) and gas into a limited working space in a short period (Aguado and Nicieza 2007; Bodziony and Lama 1996; Lama and Bodziony 1998; Mcgarr 1997). In recent years, with the advancement of technology and management, the number of coal mine accidents and deaths has shown an overall downward trend, as shown in Fig. 1. However, as deeper coal seams are mined, the possibility of occurrence of outbursts increases (Guan et al. 2009; Zhang and Kling 2006) and remains unpredictable. Improving the prediction and prevention of these underground hazards is one of the most crucial breakthroughs in mining activities, as recent outbursts have caused substantial casualties (e.g., the 2019 Fenghuangling outburst, Hunan Province, China; 13 casualties) and highlighted our limitations to mitigate sudden underground hazards (Guan et al. 2009; Yang et al. 2018). Hence, it is critical to conduct in-depth studies of the mechanism that produces outbursts.

Since the first scientific investigation of the mechanism of outbursts in 1852, a large number of experimental studies and numerical simulations have deepened our understanding of the outburst process (Beamish and Crosdale 1998). The fundamental mechanism underlying an outburst has been described by Lama and Bodziony (1998), Guan et al. (2009), Skoczylas and Ijrmms (2012), Fan et al. (2017), Jin et al. (2018), and Lei et al. (2021), forming scientific basis to current research. Among these previous studies, the multiple-factor model is the most widely recognized. This model states that an outburst is the result of the combined influence of stress, coal gas, and coal properties, playing different roles during the four stages of the dynamic process of an outburst (see Fig. 2) (Hu et al. 2008; Jin et al. 2011; Kursunoglu and Onder 2019; Lei et al. 2021).

In the outburst development stage, the coal breaks into disconnected fragments even producing coal powder that is suspended within an expanding gas phase. Usually, the coal will be ejected in the form of a spherical shell, leaving a series of fracture textures (known as coal spallation). However, due to technical limitations, the features behind outburst holes are seldom recorded. Recently, with advanced technology, laboratory simulations are often employed to fully reveal the features behind outburst holes. Among those features, coal spallation is a commonly observed result (Guo 2014; Tu et al. 2016, 2018), as indicated in Fig. 2. The formation of coal spallation can be explained using one of the three following mechanisms:

1. Dominance of gas pressure and stress distribution: according to the spherical shell destabilization hypothesis (Jiang and Yu 1995), coal spallation is controlled by the stress distribution of the cavity wall and the tensile failure of coal that occurs due to the presence of high-pressure gas in the pores and cracks.
2. Dominance of crushing wave: The crushing wave theory (Khristianovich 1953) states that coal spallation may be

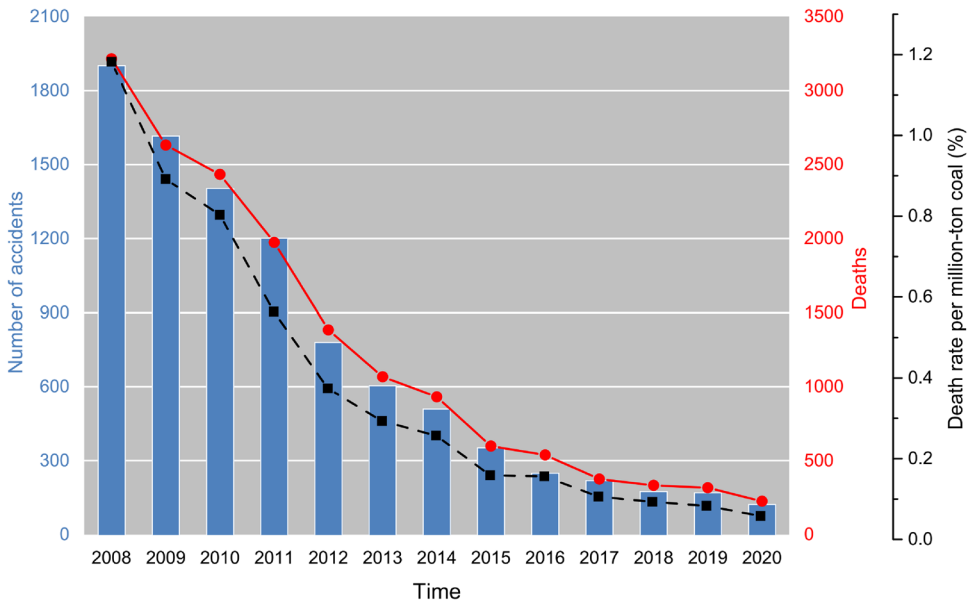

Fig. 1 Statistics of coal mine accidents in China from 2008 to 2020

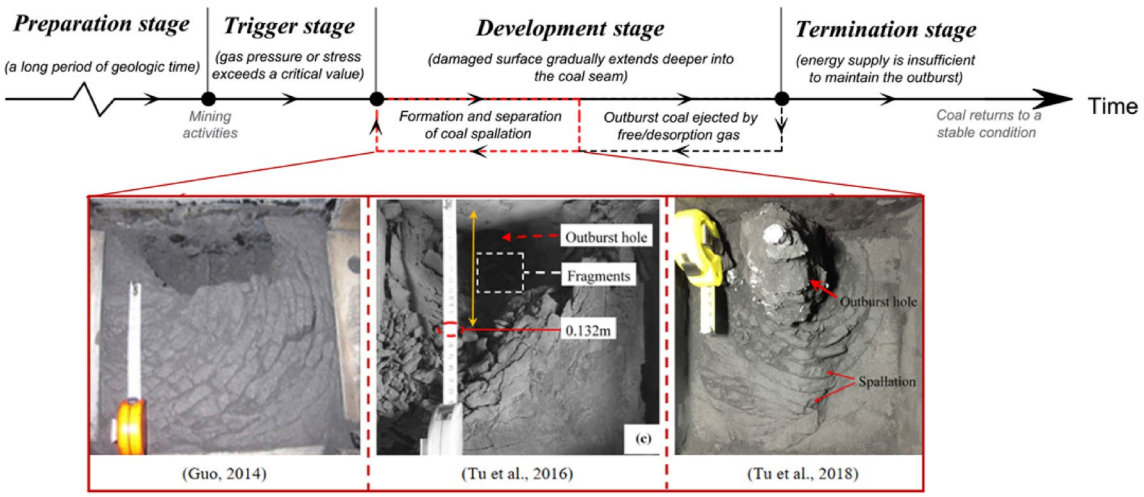

Fig. 2 Stages of the dynamic outburst process (Guo 2014; Tu et al. 2016, 2018; Lei et al. 2021)

produced by waves that are generated by the unloading of geo-stress during the outburst process. Moreover, Litwiniszyn (1983) suggested that coal spallation may be produced by sparse waves (even shock waves) that occur due to the phase transformation of coal to generate a multiphase medium in certain conditions.

3. Dominance of bearing pressure: when an outburst or impact earth pressure occurs, the geo-stress that is perpendicular to the direction of the exposed surface is unloaded, whereas the geo-stress parallel to the direction of the exposed surface increases forming a bearing pressure. This process causes crack extension along the exposed surface, i.e., spallation phenomenon (Mcgarr 1997; Vardoulakis 1984).

Regarding the mechanism of spallation formation, most studies use stress as a necessary condition, whereas the role of coal gas is considered to be limited. This may be partially correct considering that the release of strain energy can indeed lead to fracture development. However, the above models cannot explain, among other observations, the reason for the occurrence of coal spallation under stress-free conditions and why the characteristics of coal spallation are closely related to gas pressure rather than stress (Guo 2014; Tu et al. 2016, 2018) (as stress is considered the main factor controlling spallation formation).

Recently, Tu et al. (2018) theoretically analyzed the failure processes behind outbursts and indicated that a spallation would be formed when the difference in gas pressure near the exposed surface is sufficient to overcome the tensile strength, which emphasizes the role of coal gas. In fact, many studies on the principle of outburst energy imply that the effect of gas desorption plays a decisive role on the promotion of outburst. Jin et al. (2018) simulated outbursts using CO_2 and N_2 as a coal gas to investigate the role of gas desorption on an outburst coal–gas flow and concluded that the contribution of desorbed gas increased the outburst energy by 1.30–2.43 times. Tu et al. (2016) replaced coal with activated carbon in their outburst experiments and indicated that the participation of desorbed gas in the gas-enriched area increased the outburst energy by 2.68–2.88 times. Zhao et al. (2016) theoretically analyzed the development stage of the Zhongliangshan outburst and indicated that due to the initial rapid desorption capacity of coal powder in the coal–gas flow, the contribution of desorbed gas to coal transportation was approximately 6.3 times larger than contribution of free gas. However, the relationship between outburst energy and spallation formation remains unclear.

In short, although abundant results have been obtained, a theory that can feasibly explain the formation of coal spallation remains elusive; thus, it is impossible to comprehensively understand the outburst process due to its complexity. To reveal the mechanism of outbursts, we carried out a series of outburst experiments under different gas pressures using several types of gases, including carbon dioxide (CO_2), nitrogen (N_2), and helium (He). Notably, in our previous work (Lei et al. 2021), we have used a similar experimental method to investigate the energy principle of outbursts, which analyzed the impact of energy sources on outburst features and emphasized the contribution of desorbed gas. However, the formation mechanism of some features (such as the mass distribution of the ejected coal and coal spallation area) remains unclear. This study, therefore, aims to link the different expressions of outburst factors (especially gas desorption) with the evolution of coal spallation, and most importantly, to propose a viable outburst mechanism based on spallation properties. The remainder of the manuscript is organized as follows. Section 2 describes the experimental

methods used in the study, and Sect. 3 presents the results. A thorough discussion of the results is provided in Sect. 4, and finally, the conclusions are presented in Sect. 5. Through the experimental investigations, distinct properties of the coal spallation area were revealed for the first time. The present results may contribute to the understanding of the precise mechanism of an outburst and allow better promotion of mine safety.

2 Experimental Methods

2.1 Materials and Specimen Preparation

Coal was collected from the No. 10 coal seam at the Sijiazhuang Coal Mine in Shanxi Province, China. We prepared approximately 300 kg of coal for the outburst experiments. To determine the influence of gas desorption on an outburst, we altered the adsorption of the experimental gas, an effective method used in previous studies (Jin et al. 2018; Lin et al. 2018). For safety reasons, N_2 and CO_2 were used in place of explosive methane (CH_4). Since the equilibrium adsorption capacity of N_2 for coal is usually only 13.5–29.2% of the adsorption capacity of CO_2 under the same conditions (Busch et al. 2006; Cui and Zhang 2005; Sakurovs et al. 2012), it is reasonable to define CO_2 and N_2 as strong and weak absorbable gases, respectively. In addition, to rule out the influence of gas ad-/desorption, controlled experiments were conducted using He. The different initial gas desorption characteristics of the CO_2 and N_2 tests are shown in Fig. 3. The desorbed gas volume of the CO_2 tests in the first 5 s was 3.86 times higher than that of the N_2 tests, and this gap persists (although showing a decreasing trend) over time. In this case, the link between outburst development and the amount of gas desorption can also be shown.

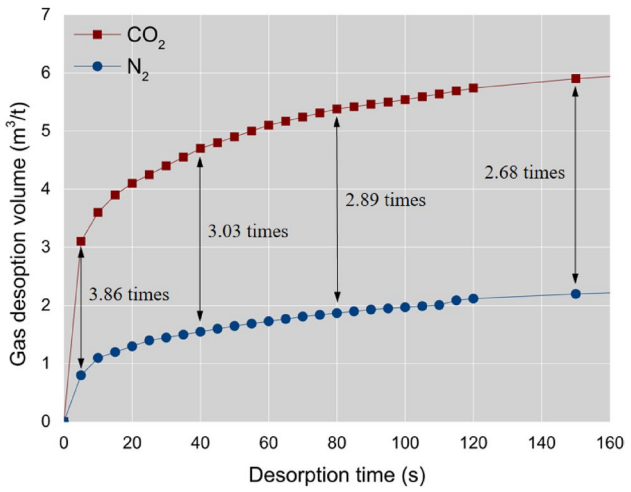

Fig. 3 Initial gas desorption characteristics of the CO_2 and N_2 tests (equilibrium pressure: 0.5 MPa)

As in most previous experimental studies, molded coal with controllable parameters was used, instead of raw coal for outburst experiments. The specimens were molded in an outburst simulation experiment chamber. The molding pressure was 60 MPa, which was applied for 40 min. To obtain the basic parameters of the experimental materials, proximate analyses, an adsorption isotherm test (at 298 K), and a pressured-mercury test were conducted. The adsorption constants a and b for CO_2 and N_2, porosity ϕ, density, proximate analyses, uniaxial compressive strength (R_c), and tensile strength (σ_t) of the materials are listed in Table 1. Taking into account statistical data, the tensile strength of intact coal is usually 1–20 MPa, while tectonic coal's tensile strength is 0.2–8 MPa (Cheng and Pan 2020). The molded coal sample ($\sigma_t = 0.4$MPa) in our experiments could, thus, be considered to have physical properties similar to tectonic coal (Skoczylas et al. 2014; Tu et al. 2016).

2.2 Experimental Equipment and Procedure

As shown in Fig. 4 (Lei et al. 2021), triaxial coal and gas outburst simulation systems (Guo 2014; Tu et al. 2016, 2018) are composed of a gas injection/vacuum pumping system (using ZJP-30 Roots vacuum pump); a loading system YAW-5000 manufactured by SUNS, China; a self-design temperature control system (composed of electrical resistance and thermal insulation materials); a self-design outburst simulation experiment chamber (internal size is 0.25 m × 0.25 m × 0.25 m); and a data collection system (composed of a data acquisition card USB-6008 manufactured by National Instruments, USA, an up to 2000 Hz high-frequency pressure transmitter TXZ11 manufactured by Taixin Instruments, China, and a 1000 fps high-speed camera). The loading system was able to apply an independent uniformly distributed load in the x, y, and z directions, where $\sigma_z \leq 80$ MPa and σ_x and $\sigma_y \leq 27$ MPa. The experimental parameters are listed in Table 2, and the main steps of the outburst experiments are as follows:

1. The primary coal was first broken into pulverized coal with a particle size of < 0.5 mm and mixed with 5% water, after which no less than 20 kg was placed into the experimental chamber;
2. A molding pressure of 60 MPa was applied to the coal for 40 min;
3. The molded coal in the chamber was kept in a vacuum for 24 h, then was filled with the corresponding gas for more than 48 h to achieve gas saturation;
4. Under the specified gas pressure (Table 2), the outburst port was opened (Fig. 4) to produce an outburst;
5. The resulting outburst hole was filled with polyurethane;

Table 1 Basic parameters of the experimental materials

Materials	Particle size (mm)	Adsorption constants (CO_2)		Adsorption constants (N_2)		Density		Proximate analysis (%)			φ(%)	Compressive strength (*MPa*)	Tensile strength σ_t (MPa)
		V_L(m^3/t)	P_L(MPa^{-1})	V_L(m^3/t)	P_L(MPa^{-1})	True density (t/m^3)	Apparent density (t/m^3)	M_{ad}	A_{ad}	V_{ad}			
Coal (anthracite)	< 0.5	58.78	1.44	19.72	0.89	1.47	1.4	4.61	6.24	7.00	4.79	2.5	0.4

6. The characteristics of the spallation were recorded;
7. The ejected coal was carefully collected at 1 m intervals and weighed.

3 Results

3.1 Characteristics of Spallation and Outburst Hole

Coal spallation represents a unique failure type for coal, and its formation process is related to multiple concurrent processes that occur during an outburst, including stress transfer, gas migration, and changes in mechanical behavior (Tu et al. 2018; Zhao et al. 2017). The most important experimental result (Fig. 5) of this study is that a spallation area can develop spontaneously during CO_2 and N_2 (absorbable gases) tests, whereas the outbursts caused by the He (non-absorbable gas) tests cannot produce a spallation area. This result further indicates that a spallation area is not an inevitable result of an outburst. Moreover, the development of an outburst may follow a different mode depending on the effect of gas desorption (discussed in Sect. 4.1).

The characteristics of a spallation area were as follows: the spallation area was centered at the outburst port and developed into a spherical shell shape, generally with a certain thickness. When comparing the results of Experiments # 2–9 and # 3–8, the spallation phenomena in the CO_2 tests were more evident than those in the N_2 tests, indicating that an increase in gas adsorption capacity contributes to the development of spallation.

Figure 6 shows the polyurethane molds made of the outburst holes produced in the outburst tests. The comparison of the models indicates that the hole shapes may vary. In the CO_2 tests, the upper parts of the holes were cylindrical, and the lower parts were tapered; the radius of the upper parts were approximately twice the radius of the lower parts of the holes. In the N_2 tests, the holes were cone shaped, whereas in the He tests, the holes were approximately hemispherical.

3.2 Outburst Intensity

The results (Table 3) of the outburst tests show that there is a gas pressure threshold required to produce an outburst. When the gas pressure exceeds this threshold, an outburst occurs. The threshold values were 0.35–0.4 MPa for the CO_2 tests, 0.4–0.45 MPa for the N_2 tests, and 0.45–0.5 MPa for the He tests, indicating that the pressure threshold decreases as the amount of adsorbed gas stored in the coal increases. The main cause for this phenomenon may be attributed to the decreased coal strength induced by gas adsorption (Cheng and Pan 2020).

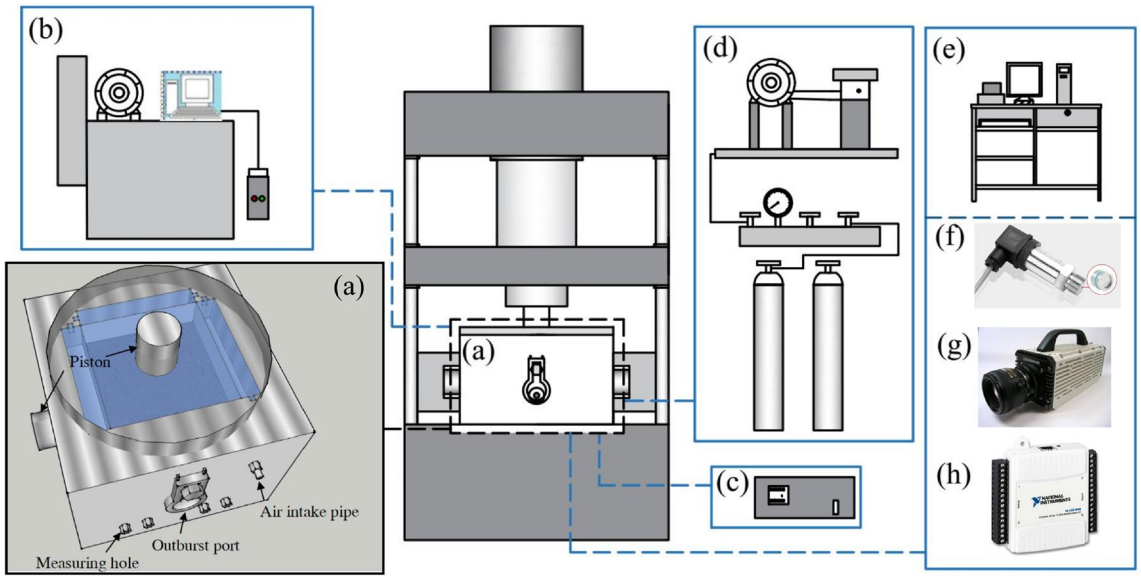

Fig. 4 Schematic diagram showing the arrangement of the triaxial coal and gas outburst simulation system (Guo 2014; Tu et al. 2018; Lei et al. 2021): **a** outburst simulation experimental chamber, **b** loading system, **c** temperature control system, **d** gas injection/vacuum pumping system, **e** data collection system, **f** an up to 2000 Hz high-frequency pressure transmitter, **g** a 1000 fps high-speed camera, and **h** a data acquisition device

Table 2 Experimental scheme of coal and gas outburst tests

Experiment number	Gas type	Gas adsorption	Gas pressure (MPa)	Ambient temperature (°C)	Triaxial stress ($\sigma_x = \sigma_y = \sigma_z$, MPa)
# 1 − *i* (*i* = 1,2,3…*n*)	He	None	0.1–0.7	25	0
# 1–1*	He	None	0.6	25	5
# 2-i (*i* = 1,2,3…*n*)	N_2	Weak	0.1–0.7	25	0
# 2–1*	N_2	Weak	0.5	25	5
# 3-i (*i* = 1,2,3…*n*)	CO_2	Strong	0.1–0.7	25	0
# 3–1*	CO_2	Strong	0.5	25	5

To accurately evaluate the destructiveness of an outburst under equivalent external conditions, the relative outburst intensity (RIO), which is related to the volume of coal masses with outburst risk has been widely adopted (Jin et al. 2018; Wang et al. 2018). As shown in Fig. 7, the RIO values of the experiments exhibited near-linear increasing trends as the outburst pressure increased. The growth proportion also increased as the adsorption capacity of the experimental gas increased (the amplitude increase ranges from 10.71 to 18.80%). Moreover, comparing the results from the outburst experiments (using CO_2 and N_2) and the controlled experiments (using He) under the same outburst pressure, shows that the gas desorption increased the outburst distance and the RIO by 19.75–75.73% and 48.44–135.40%, respectively, indicating that gas desorption from coal can enhance the intensity and destructiveness of the outburst.

3.3 Characteristics of the Outburst Coal

In this study, ejected coal was carefully collected at 1 m intervals and weighed after each experiment. As shown in Fig. 8, with an increase in gas adsorption capacity, the mass and distance of the ejected coal both increased. Importantly, we also observed a wave-shaped distribution of the ejected coal (Fig. 8a), and its mass distribution also had fluctuations similar to the peaks and troughs of a waveform (Fig. 8b). This phenomenon has also been mentioned in previous studies (Guo 2014; Zhao 2017; Lei 2021). It may indicate that in the development stage of an outburst, the gas pressure gradient behind the exposed

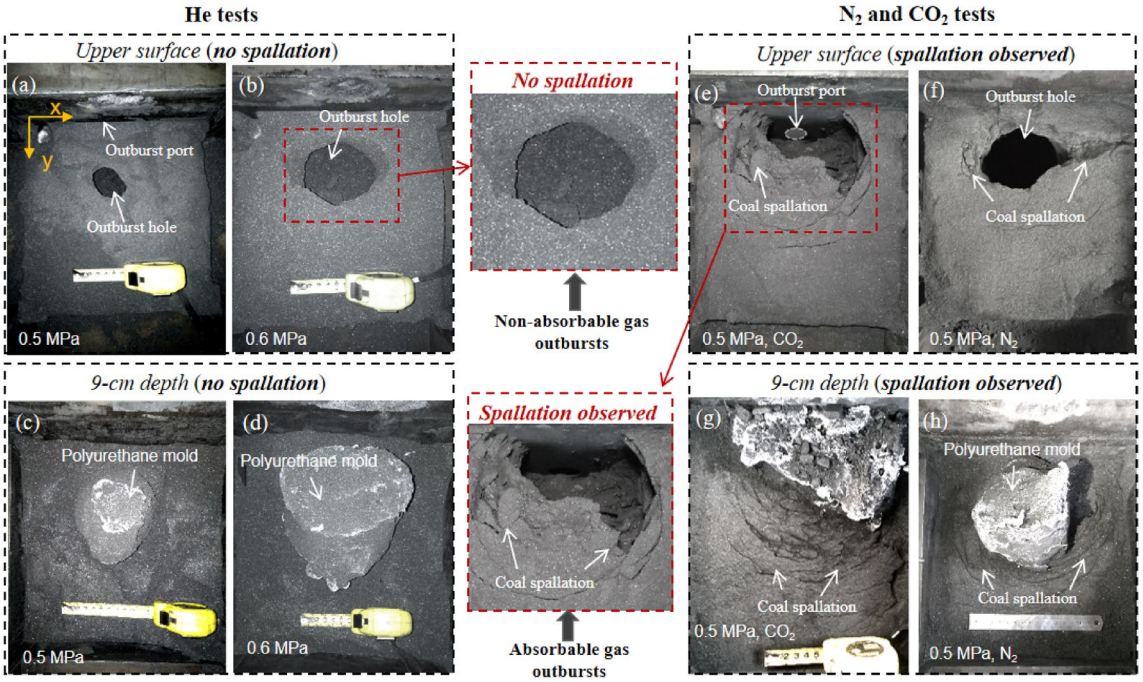

Fig. 5 Characteristics of spallation and the hole: **a** and **c** Experiment # 1–9 (0.5 MPa, He); **b** and **d** Experiment # 1–10 (0.6 MPa, He); **e** and **g** Experiment # 2–9 (0.5 MPa, CO_2); **f** and **h** Experiment # 3–8 (0.5 MPa, N_2)

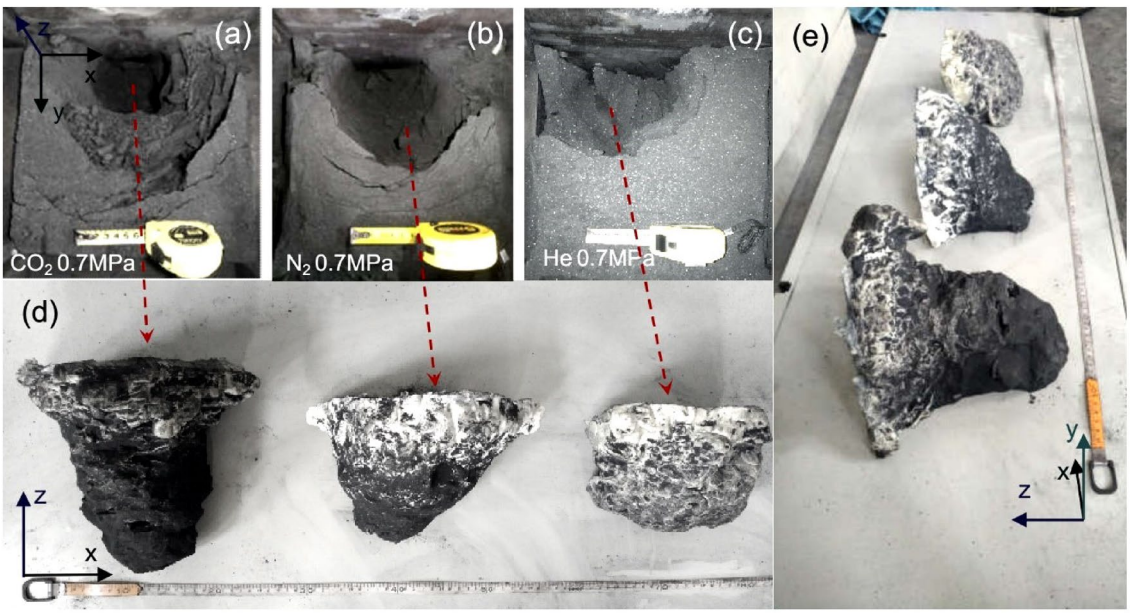

Fig. 6 Polyurethane molds of the outburst holes produced: **a** Experiment # 3–10; **b** Experiment # 2–11; **c** Experiment # 1–11; **d** polyurethane molds of the outburst holes; and **e** side view of the molds

surface causes the outburst coal to exhibit periodic ejection, resulting in the ejected coal mixing with outburst gases to form various types of coal–gas flow (e.g., suspension flow, stratified flow, dune flow, and plug flow). In other words, the periodic development of coal spallation may eventually lead to a wave-shaped distribution of the ejected coal. This is discussed further in Sec. 4.2.

Moreover, the mass distributions of coal ejected in the N_2 and CO_2 tests were more likely to be concentrated farther from the outburst port when compared to the He tests, which

Table 3 Results of the coal and gas outburst simulation experiments

Experiment number	Type of gas	Gas pressure (MPa)	Results of outburst	Mass of filled coal (kg)	Intensity of outburst (kg)	Relative intensity of outburst (%)	Distance of outburst (m)
# 1–1 ~ # 1–8	He	0.1–0.45	No outburst	–			
# 1–9	He	0.5	Outburst	21.012	2.170	10.327	10.3
# 1–10	He	0.6	Outburst	20.854	2.355	11.293	15.4
# 1–11	He	0.7	Outburst	20.933	2.649	12.655	16.2
# 1–1*	He	0.6	Outburst	21.421	2.754	12.857	16.8
# 2–1 ~ # 2–7	N_2	0.1–0.4	No outburst	–			
# 2–8	N_2	0.45	Outburst	20.566	2.791	13.571	16.0
# 2–9	N_2	0.5	Outburst	21.051	3.027	15.329	17.1
# 2–10	N_2	0.6	Outburst	20.119	3.421	17.003	18.5
# 2–11	N_2	0.7	Outburst	21.201	3.992	18.829	19.4
# 2–1*	N_2	0.5	Outburst	21.054	3.577	16.988	17.2
# 3–1 ~ # 3–6	CO_2	0.1–0.35	No outburst	–			
# 3–7	CO_2	0.4	Outburst	20.779	3.721	17.908	17.2
# 3–8	CO_2	0.5	Outburst	20.956	4.881	23.292	18.1
# 3–9	CO_2	0.6	Outburst	21.036	5.342	25.394	21.8
# 3–10	CO_2	0.7	Outburst	20.211	6.020	29.790	24.9
# 3–1*	CO_2	0.5	Outburst	20.197	5.280	26.144	

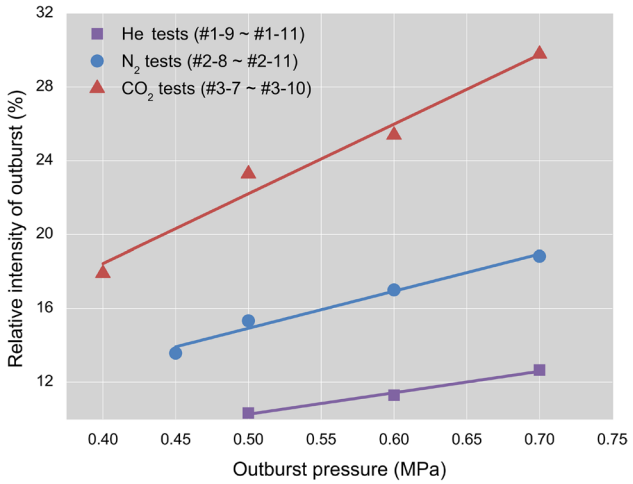

Fig. 7 Relative intensities of the coal outbursts at different pressures

indicates that gas desorption had a significant effect on the outburst coal–gas flow. This resulted in a greater ejection distance and a stronger conveying capacity of the ejected coal, as well as increased destructiveness.

3.4 Outburst Experiments with Applied Triaxial Stress

Outburst experiments with applied triaxial stress were conducted to thoroughly understand the effect of stress. The triaxial loading pressures for σ_x, σ_y, and σ_z were 5 MPa, based on field-monitoring data for coal pillar loading; that is, σ_z was approximately 0–10 MPa, and the confining pressure was approximately 4 MPa (Medhurst and Brown 1998). As shown in Fig. 9a, the results of Experiment # 1–1* are consistent with the results of Experiment # 1–10 (Fig. 5f), as no spallation was observed, which suggests that stress conditions are not the key factors that produce a spallation area.

Nevertheless, the results of Experiment # 2–1* (Fig. 9b) and # 3–1* (Fig. 9c) revealed that the width of the spallation area increased (8.91–14.45%) compared to the experiments without applied stress (Fig. 5g, h), indicating that additional stress can promote the development of a spallation area. Moreover, according to Table 3, the additional stress applied increased the outburst distance and relative intensity of outburst (RIO) by 0.58–11.60% and 10.82–13.85%, respectively, which further demonstrates that the intensity and extent of destruction of the outburst were affected by the stress. Briefly, the experiments indicate that gas ad-/desorption is extremely critical for the occurrence of a spallation area. In contrast, stress only promotes the development of a spallation area.

3.5 Characteristics of Spallation Thickness

After each outburst experiment, we recorded the number of spallation areas and the spallation thickness (the distance between two adjacent spallation areas) at different depths. In Fig. 10, L represents the distance from the spallation to the exposed surface, and H represents the depth of the molded

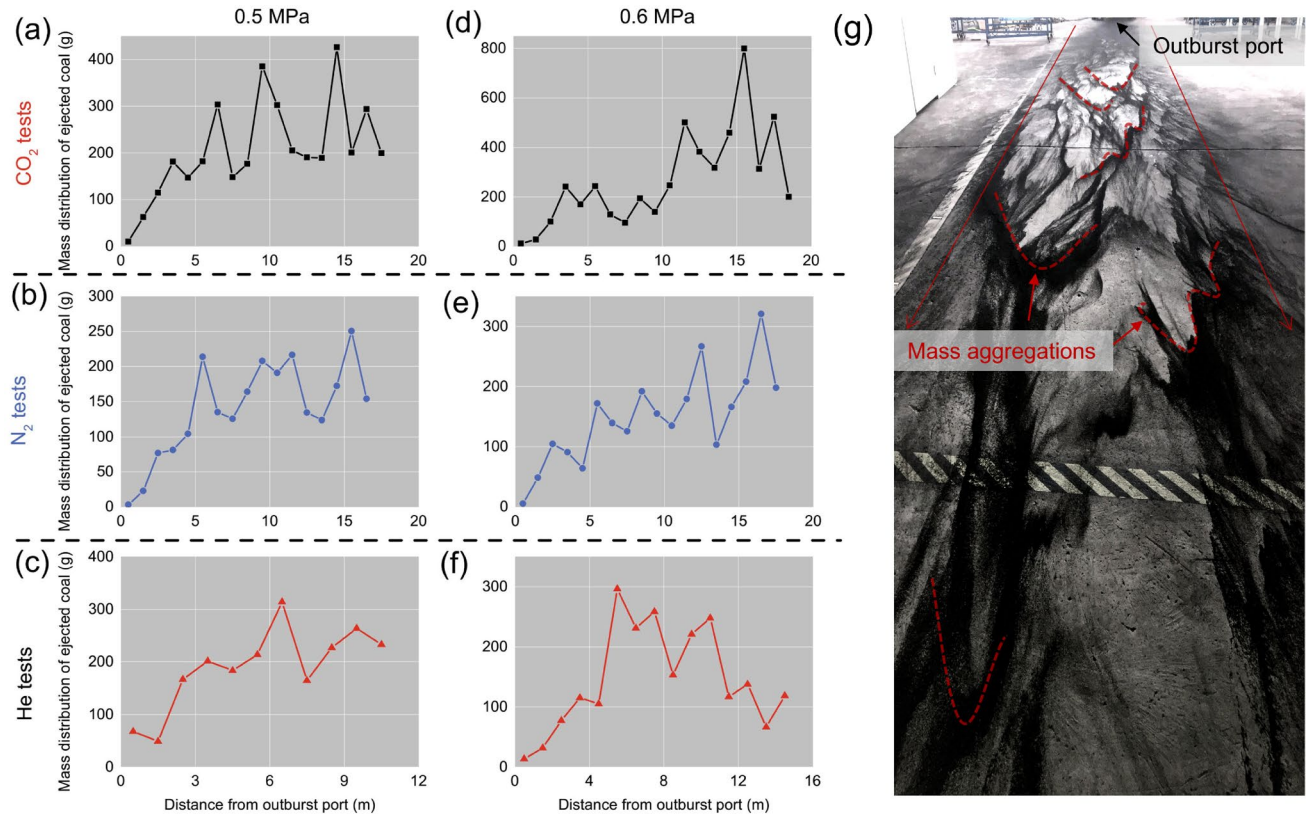

Fig. 8 Characteristics of the ejected coal from the outbursts: **a** Experiment # 3–8 (CO_2, 0.5 MPa); **b** Experiment # 2–9 (N_2, 0.5 MPa); **c** Experiment # 1–9 (He, 0.5 MPa); **d** Experiment # 3–9 (CO_2, 0.6 MPa); **e** Experiment # 2–10 (N_2, 0.6 MPa); **f** (Experiment # 1–10 (He, 0.6 MPa); and **g** deposited coal examples

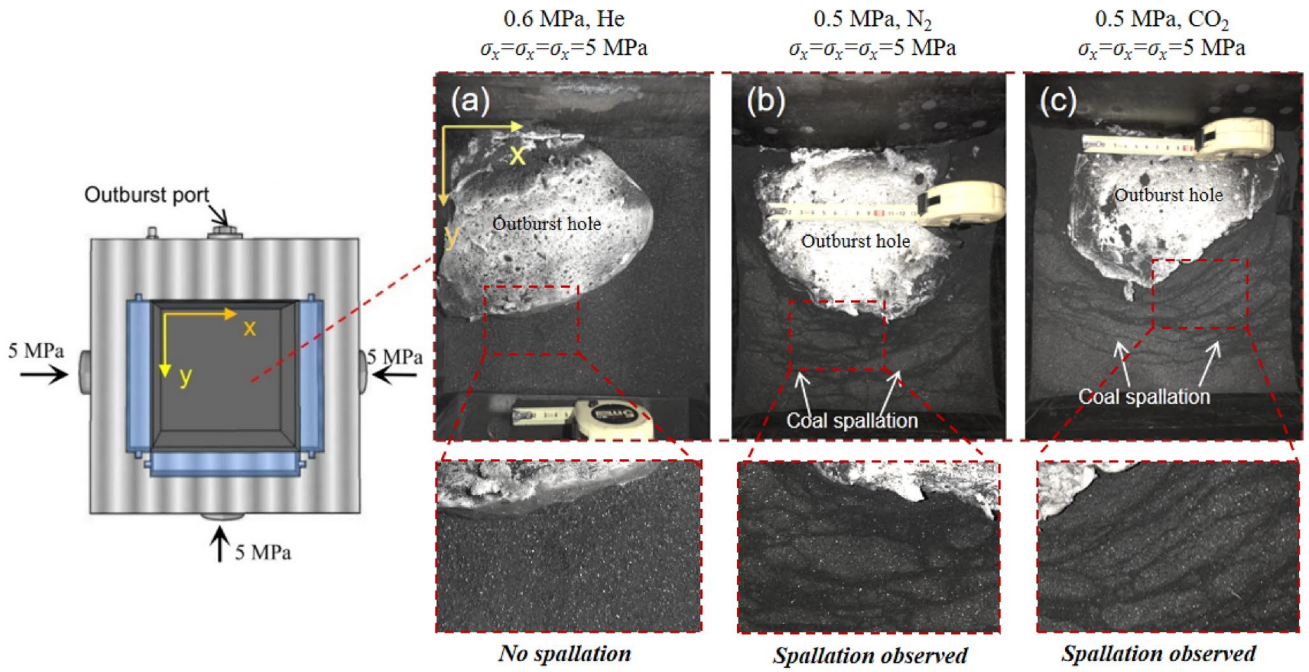

Fig. 9 Effects of triaxial stress on spallation formation: **a** Experiment # 1–1* (He, 0.6 MPa, $\sigma_x = \sigma_y = \sigma_z = 5$MPa); **b** Experiment # 2–1* (N_2, 0.5 MPa, $\sigma_x = \sigma_y = \sigma_z = 5$MPa); **c** Experiment # 3–1* (CO_2, 0.5 MPa, $\sigma_x = \sigma_y = \sigma_z = 5$MPa)

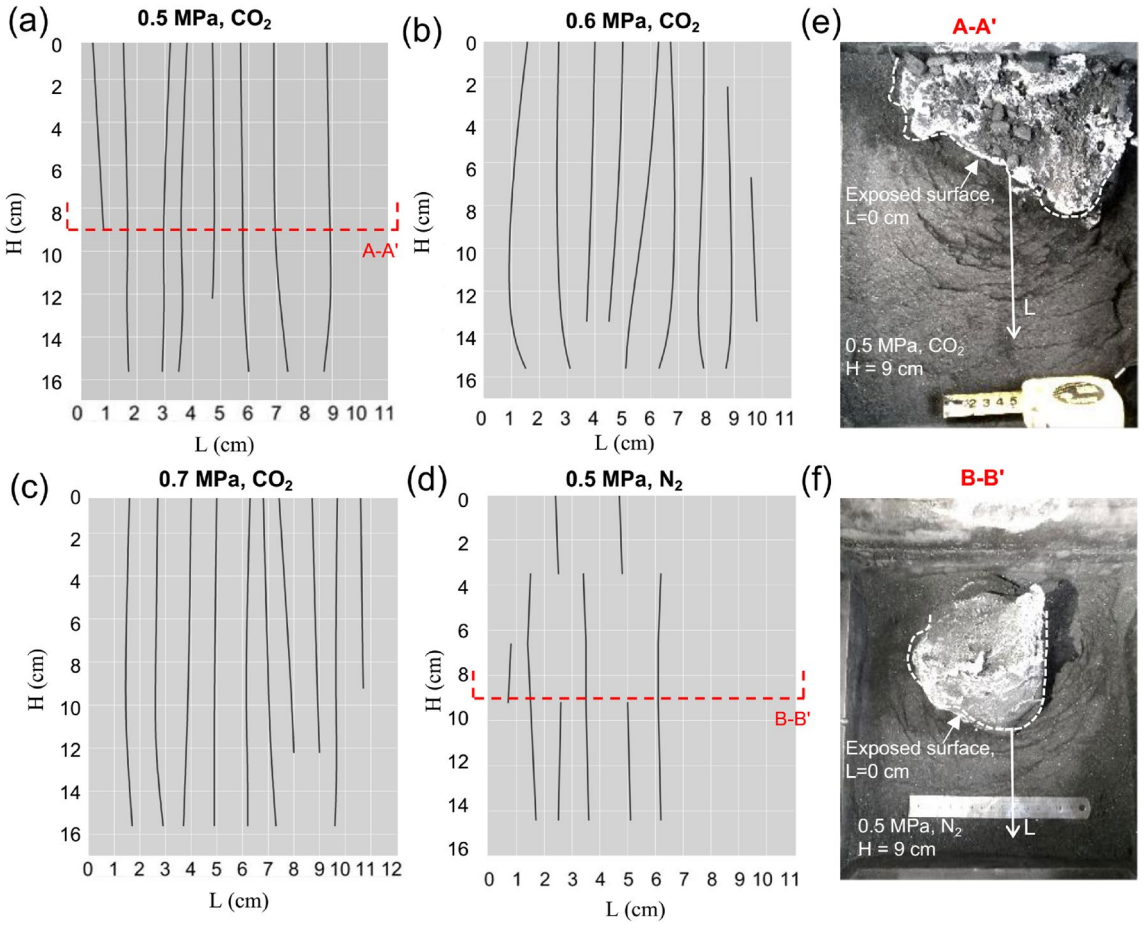

Fig. 10 Relationships between the distance from the spallation to the exposed surface (L) and the depth of the coal spallation (H): **a** Experiment # 3–8 (CO_2, 0.5 MPa); **b** Experiment # 3–9 (CO_2, 0.6 MPa); **c** Experiment # 3–10 (CO_2, 0.7 MPa); **d** Experiment # 2–9 (N_2, 0.5 MPa); and **e** and **f** spallation phenomenon at H = 9cm in Experiment # 3–8 and Experiment # 2–9

coal. The experimental results show that for the same gas, spallation thickness remained unchanged with changing outburst pressure and remained almost constant with increased L or H. For the tests under the same outburst pressure, the stronger the adsorption capacity of the experimental gas, the smaller the spallation thickness (1.09 cm for CO_2 tests and 1.13 cm for N_2 tests). The results indicate that gas desorption may be a key factor affecting the characteristics of spallation thickness.

Moreover, the width of the spallation area (L_0) can be determined from the maximum value of L. By comparing Experiments # 3–8 and # 2–9, the average thickness obtained in the CO_2 tests was slightly smaller (0.96 times) than the thickness obtained in the N_2 tests, whereas the L_0 of the CO_2 tests was much larger (1.71 times) than that of the N_2 tests. In addition, by comparing Experiments # 3–10 and # 3–8, an increase in outburst pressure can increase L_0 by 1.22 times. This indicates that, with the effect of gas desorption, the width of the spallation area can be significantly increased, whereas the spallation thickness is less affected.

3.6 Characteristics of Gas Pressure Changes

The characteristics of changes in gas pressure are shown in Fig. 11, where we define the instantaneous pressure drop rate (v_p, MPa/s) as the pressure difference in 0.02 s intervals. The pressure drops during the outbursts were 0.2089–0.2390 MPa/s for the CO_2 tests, 0.3811–0.4570 MPa/s for the N_2 tests, and 0.5669–0.6281 MPa/s for the He tests. As the gas adsorption ability increases, the average pressure drops more slowly, thereby extending the duration of the outburst process (increased by 1.37–2.71 times). This indicates that gas desorption effectively resisted the pressure drop during the outburst, which is consistent with previous studies (Guo 2014; Lei et al. 2021).

In addition, comparing the differences in the pressure drop rates (v_p) between absorbable gas outbursts (CO_2 and N_2 tests) and non-absorbable gas outbursts (He tests), their tendencies were similar, characterized by an initial increase and then a decrease. As indicated in Fig. 11b, the

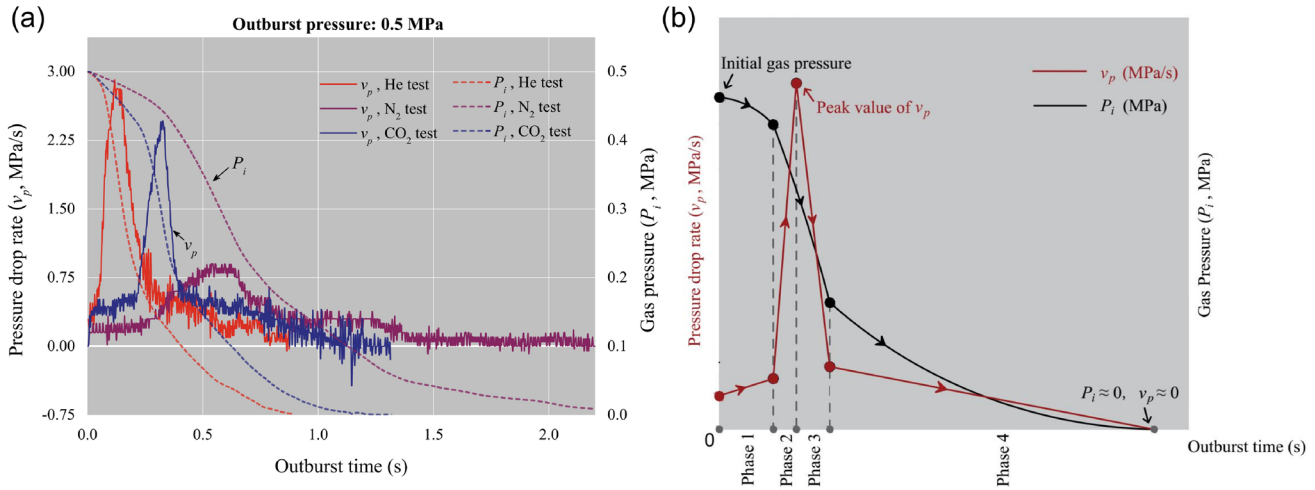

Fig. 11 Characteristics of the pressure changes during an outburst: **a** changes in gas pressure (P_i, relative pressure) and instantaneous pressure drop rate (v_p); **b** plot of the characteristics of the gas pressure changes through the 4 phases of the outburst

characteristics of changes in gas pressure during the experiments fall into one model. Phase 1 (stable phase): when an outburst occurs, the gas pressure begins to drop and v_p rises steadily; Phase 2 (acceleration phase): v_p increases rapidly (point B_1) and reaches its maximum (point B_2) following a 2.4–4.9 times increase within 0.09–0.14 s; Phase 3 (deceleration phase): v_p rapidly drops to a value (point B_3) close to point B_1 within 0.08–0.12 s; Phase 4 (stable phase): v_p slowly decreases, and the gas pressure gradually approaches the ambient pressure. In the outburst process, v_p reaches its maximum when the gas pressure drops to approximately 2/3 of the outburst pressure, indicating that the outburst may have entered the most violent moment and gradually begins to weaken. This is discussed further in Sec. 4.2.

However, for absorbable gas outbursts, especially CO_2, the peak value f v_p (Fig. 11a) was significantly smaller than that of the He tests. This demonstrates that gas desorption in the coal seam could limit the increase in the pressure drop rate, thereby limiting the drastic pressure drop. This ability increases with an increase in the adsorption capacity.

4 Discussion

4.1 Mechanism of Coal Spallation Formation

Coal spallation is a common aftermath of an outburst, and most existing theories postulate that the emergence of a spallation area is mainly controlled by stress rather than coal gas (Bodziony and Lama 1996; Cao et al. 2001; Tu et al. 2018). However, our experiments show that outbursts induced by absorbable gases can produce spallation areas in the molded coal, whereas outbursts induced by non-absorbable gases cannot. This laboratory result necessitates a model to show the influence of coal gas in the outburst development stage, especially its unique contribution to the formation of a spallation area.

4.1.1 Formation of Coal Spallation Area

The final failure type for coal is tensile failure, and its key mechanical conditions can be expressed by Eq. (1) (An et al. 2013; Skoczylas et al. 2014; Tu et al. 2018). In this case, the occurrence of coal spallation determined by whether the gas pressure difference ($P_i - P_a$) near the exposed surface exceeds the tensile strength (σ_t). Moreover, considering that coal failure under tensile stress can be attributed to tensile micro-cracks, the formation of coal spallation during outbursts can be roughly described, as shown in Fig. 12. Thus, the pressure gradient behind the exposed surface acts as a periodic physical knife that incrementally cuts the exposed coal and pushes the coal–gas flow along the cut. Consequently, we can clearly observe a wave-shaped distribution of the ejected coal (Fig. 8). Here,

$$P_i - P_a \geq \sigma_t, \tag{1}$$

where P_i is the gas pressure in the coal at the exposed surface in MPa, P_a is the ambient atmospheric pressure in MPa, and σ_t is the tensile strength of the coal, MPa.

As the development of coal spallation can be mainly attributed to a sufficient pressure gradient, it is reasonable to assume that the reason for the absence of spallation area in the He tests is because the high-pressure gradient exists only at the surface, and therefore, the formation of spallation only occurs on the exposed surface. Evidently, there is a lack of a sufficient internal pressure gradient to develop

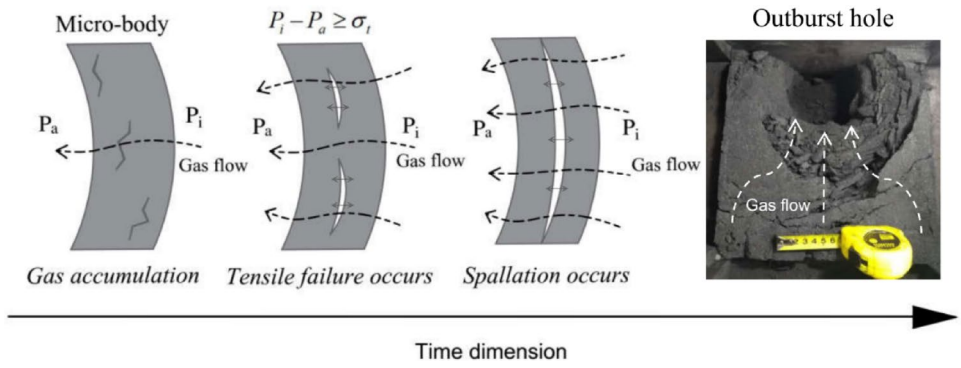

Fig. 12 The formation process of coal spallation. Free gas in small pores and the gas adsorbed in the coal are released into the crack, which leads to gas accumulation in the small crack. If the pressure gradient is high enough, the small crack will expand tangentially, and the adjacent cracks will connect to form a spherical spallation that is parallel to the exposed surface. As a result, the gas pressure gradient behind the outburst front causes the fragmented coal to be continuously ejected, and the destruction front will gradually deeper into the internal coal seams

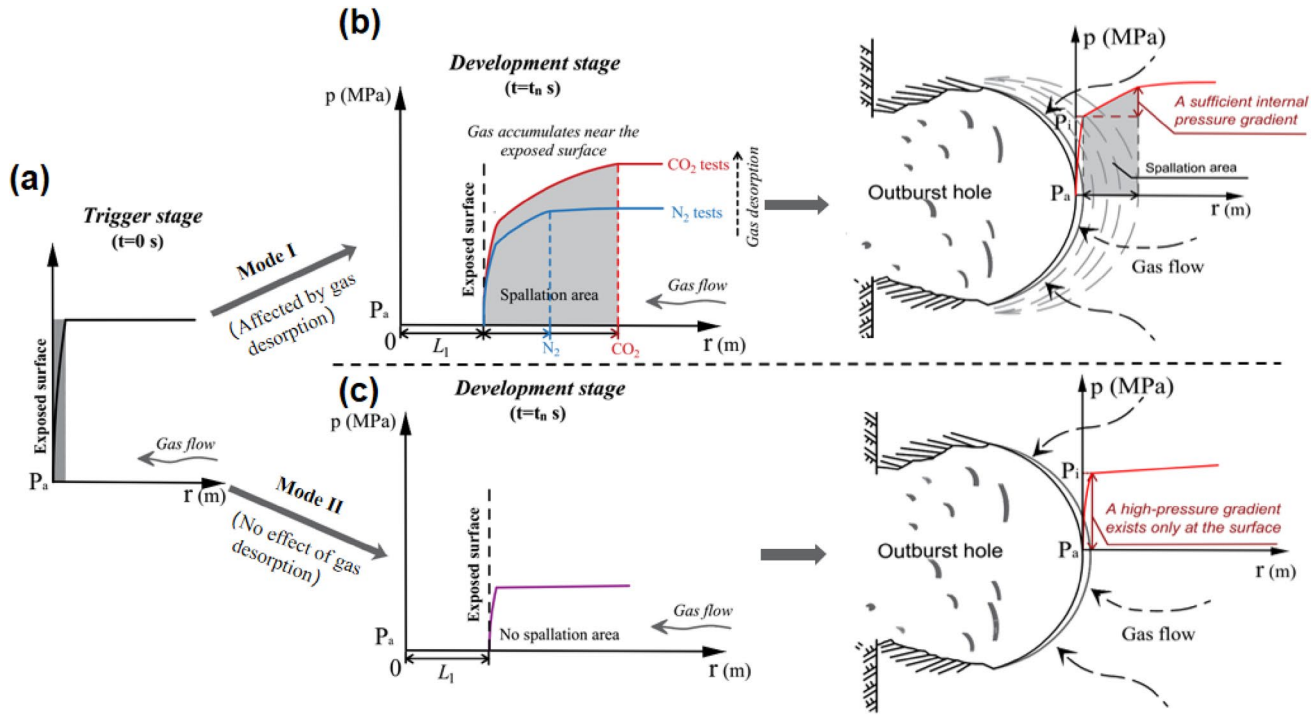

Fig. 13 Outburst development process: **a** changes in pressure gradient; **b** development process with a spallation area; **c** development process without a spallation area. L_1 represents the maximum length of the outburst hole; P_i represents the gas pressure on the exposed surface; P_a represents the ambient atmospheric pressure; and r represents the distance from the exposed surface. In Mode I, the occurrence of a spallation area is ascribed to a sufficient internal pressure gradient. In Mode II, a high-pressure gradient only exists at the surface, such that coal spallation can only occur on the surface

a spallation area. In this case, the outburst process can be divided into two modes, as shown in Fig. 13.

In Mode I (Fig. 13b), the evolution of an outburst involves three concurrent processes: (a) the formation of a spallation area ahead of the exposed surface, (b) ejection of the coal spallation, and (c) transportation of the coal–gas flow. In the evolution of an outburst, the occurrence of a spallation area is ascribed to a sufficient internal pressure gradient. Notably, as the average spallation thickness is almost constant (Fig. 10), the pressure gradient formed in the spallation area may show an approximate linear change, which is likely to be principally controlled by the mechanism of gas migration. In Mode II (Fig. 13c), the evolution of an outburst also involves three concurrent processes: (a) the formation

of coal spallation on an exposed surface, (b) ejection of the coal spallation, and (c) transportation of the coal–gas flow. Unlike Mode I, a high-pressure gradient only exists at the surface, such that coal spallation can only occur on the surface. Notably, the characteristics of the coal–gas flow in these two modes are similar (Fig. 8).

Our results suggest that the occurrence of a coal spallation area is determined by whether a sufficient internal pressure gradient can be developed near the exposed surface, which is consistent with the mechanical conditions of tensile failure (Fan et al. 2017; Litwiniszyn 1983; Tu et al. 2018; Vardoulakis 1984). The mechanical model that we propose includes significant additions to models from previous studies. In particular, the experimental results indicate that gas ad-/desorption is extremely critical for the occurrence and development of a coal spallation area. In contrast, stress conditions are not critical for the occurrence of a spallation area but can evidently promote its development. The links between these two outburst factors and coal spallation formation are discussed in the following subsections.

4.1.2 Effect of Gas ad-/Desorption on Coal Spallation Formation

Before the experiments were conducted, the molded coal in the chamber was maintained under vacuum for 24 h, and then, the chamber was filled with the specific gas (listed in Table 2) for more than 48 h. For the N_2 and CO_2 tests, when the matrix gas pressure gradually increases as the adsorption equilibrium time increases, the effective stress is reduced; however, the matrix swells (Jasinge et al. 2011; Hu et al. 2020). Although the evolution of permeability is controlled by the competing effects of these two processes, the swell of the matrix generally dominates (Pan and Connell 2007). As the adsorption time increases, the permeability gradually decreases and eventually reaches a relatively low value. Previous studies (Li et al. 2011; Long et al. 2008) have conducted many coal permeability experiments on the different adsorption characteristics of coal samples and different gases (such as CH_4, CO_2, and He) under different pore pressures, revealing that the greater the adsorption, the lower the coal permeability. The permeabilities in the CO2 adsorption tests in this study were only 18.09–54.55% of those in the controlled tests using He.

Hence, in the outburst development stage, the radial flow of gas will inevitably be inhibited due to low coal permeability caused by gas adsorption, especially in areas away from exposed surfaces. Meanwhile, the loss of initial equilibrium in adsorption and desorption behind the outburst front leads to the rapid desorption of the adsorbed gas, which favors the accumulation of gas, thereby limiting the drastic pressure drop. Consequently, gas ad-/desorption provides good conditions for the formation of an internal pressure gradient, which eventually leads to the development of spallation area. As most outbursts occur in the tectonic zone characterized by gas enrichment, low strength, and low permeability ($10^{-19} - 10^{-16}\mathrm{m}^2$) under in-situ stress (Cheng and Pan 2020), the conditions required for Mode I are universal. A coal spallation area is therefore an overall evident outcome. When applying the two models in Fig. 13 to an actual mine, Mode I is suitable for general conditions, whereas Mode II (Fig. 13c) is only suitable for gas-poor conditions. To some extent, Mode I represents a more destructive outburst when compared to Mode II.

When comparing the different spallation characteristics between the CO2 and N_2 tests, the spallation thickness (d) and the width of the spallation area (L_0) in the CO_2 tests were both larger than those of the N_2 tests (see Fig. 10). This further indicates that, during an outburst and due to the increase in gas desorption, the internal pressure gradient increases slightly (1.76–4.42%), and its range increases significantly (43.55–66.20%).

4.1.3 Effect of Stress on Coal Spallation Formation

When the coal is exposed, the stress equilibrium is disrupted, and the stress within the coal is rapidly transferred, causing the tangential stress to become concentrated and the radial stress to decrease. With the development of outburst, coal will generally experience compressive strain, plastic failure, and tensile failure. In this process, the coal permeability evolution can be expressed as a discrete function (An et al. 2013):

$$k = \begin{cases} \exp\left[\alpha\left(\Delta\Theta - 3\beta_f\left(p_f - p_0\right)\right)\right]k_0, \gamma^p > 0 \\ (1+\xi\gamma/\gamma^{p*})\exp\left[\alpha\left(\Delta\Theta - 3\beta_f\left(p_f - p_0\right)\right)\right]k_0, 0 < \gamma^p < \gamma^{p*}, \\ (1+\xi)\exp\left[\alpha\left(\Delta\Theta - 3\beta_f\left(p_f - p_0\right)\right)\right]k_0, \gamma^p \le \gamma^{p*} \end{cases} \tag{2}$$

where k is the coal permeability in m^2, α is the impact factor of the volume stress on the permeability; Θ is the volume stress, MPa; p_0 is the initial gas pressure, MPa; ξ is the jump coefficient for the coal permeability; γ^p and γ^{p*} are the softening parameter and the transition value of the softening parameter, respectively; and k_0 is the initial coal permeability, m^2.

Based on Eq. (2), as the stress increases, the coal permeability decreases when$\gamma^p = 0$, increases approximately linearly when$0 < \gamma^p < \gamma^{p*}$, and is constant when $\gamma^p \le \gamma^{p*}$. The relationship between coal permeability and the stress–strain process of coal can be described as shown in Fig. 14. Accordingly, when the coal experiences plastic failure and irreversible damage in the outburst development stage, the coal permeability increases rapidly (by approximately one to two orders of magnitude based on Eq. (2)] (Durucan and Edwards 1986; Jasinge et al. 2011),

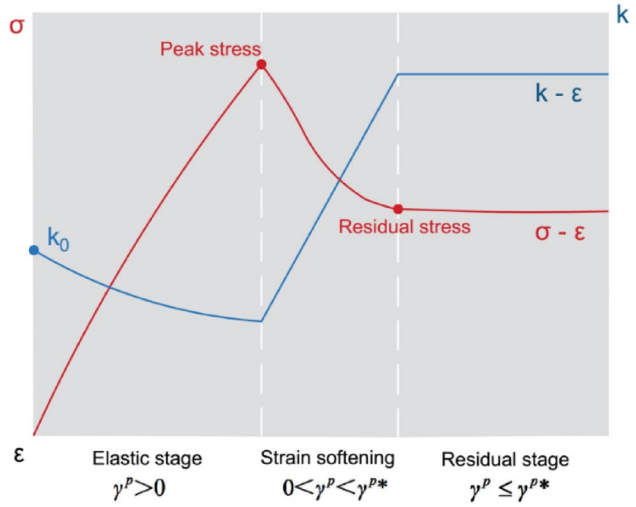

Fig. 14 Permeability evolution during the stress–strain process of coal. During outbursts, coal experiences a three stage stress–strain process (Alonso et al. 2010; Jaiswal and Shrivastva 2009). The elastic regime exists when $\gamma^p = 0$; strain softening behavior occurs if $0 < \gamma^p < \gamma^{p*}$; and the residual state begins at $\gamma^p \leq \gamma^{p*}$, where γ^p and γ^{p*} are the softening parameter and the transition value of the softening parameter, respectively

which provides optimal conditions for gas flow such that a high gas pressure gradient forms near the exposed surface. Meanwhile, the crushed coal on the exposed area can be stripped and transported away quickly due to the quick migration of the coal gas.

In addition, the experimental results show that greater stresses would produce larger spallation area widths (Fig. 10), indicating that stress conditions can promote the development of spallation. This may be attributed to the weakening of the coal induced by stress evolution, which reduces its ability to resist spallation formation.

Although previous studies have reported that spallation areas are observed following rock bursts (Lama and Bodziony 1998; Mcgarr 1997), the outburst process discussed herein is different from rock bursts, because it is mainly related to high stress within the coal. Our experiments show that outbursts can occur as long as the gas pressure reaches a certain threshold regardless of the stress conditions (see Table 3), which further demonstrates that outbursts can be regarded as gas-driven eruptions (Guan et al. 2009; Zhang and Kling 2006). Briefly, the contribution of stress evolution to spallation development can be summarized into two aspects: providing good conditions for gas flow and reducing the mechanical strength of the coal.

4.2 Development of Coal and Gas Outbursts

Coal and gas outbursts are characterized by a violent ejection of pulverized coal (rock) and abundant coal gases (Skoczylas and Ijrmms 2012; Tu et al. 2016; Wang et al. 2018; Zhao et al. 2016). To determine the relationship between coal spallation ejection and the outburst development, we made the following assumptions for the outburst process (Fig. 15a): (1) the ejected spallation is a spherical shell with a certain thickness and (2) coal–gas flow is mainly a plug flow formed by high-speed gas and ejected spallation. When we consider a solid vertical line (Fig. 15b) resulting from a single ejected spallation, then the spallation thickness is 0.0305–0.0366 m, which contradicts our observations (0.0099–0.0112 m, Fig. 10). Hence, the observed mass aggregations are the result of the accumulation of several spallation ejections.

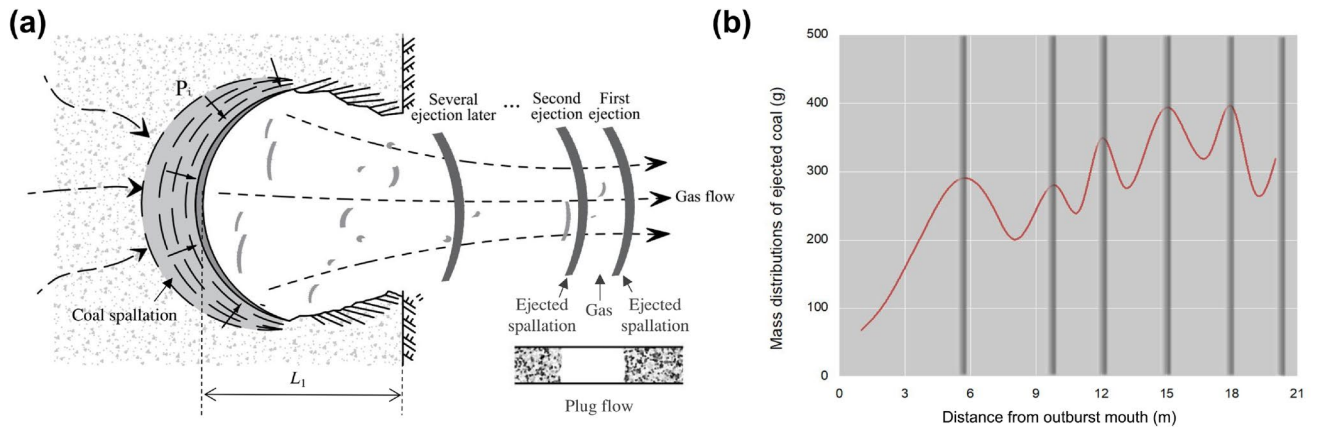

Fig. 15 Correlations between coal spallation formation and deposited coal: **a** schematic diagram showing the transport mechanism of the outbursts; **b** mass distributions of the deposited coal (Experiment # 3–8), where the mass aggregations are shown as solid vertical lines. The pressure gradient behind the outburst front controls the formation of a spallation area and causes the surface coal spallation to undergo periodic ejection, resulting in the outburst coal mixing with released coal gases to form a high-speed coal–gas flow, where a wave-shaped distribution of the ejected coal is a common result

Table 4 Parameters regarding outburst propagation

Gas type	Outburst pressure (MPa)	t(s)	L_1(m)	L_0(m)	d(m)	n_0	$\overline{v_t}$(m/s)	f_n(Hz)
He	0.5	0.532	0.122	0	≈ 0.01	12	0.229	23
He	0.6	0.564	0.131	0	≈ 0.01	13	0.232	23
He	0.7	0.598	0.145	0	≈ 0.01	15	0.242	24
N_2	0.5	0.681	0.166	0.062	0.0102	16	0.244	24
N_2	0.6	0.712	0.183	0.067	0.0103	18	0.257	25
N_2	0.7	0.784	0.213	0.071	0.0099	22	0.258	27
CO_2	0.5	0.745	0.192	0.089	0.0109	18	0.258	24
CO_2	0.6	0.771	0.211	0.104	0.0111	19	0.274	25
CO_2	0.7	0.821	0.245	0.118	0.0108	23	0.298	28

t represents the total time of the coal ejection process recorded by the high-speed camera, which is different from the outburst duration shown in Fig. 11

Table 4 lists the parameters regarding outburst propagation, among which t represents the outburst time and was recorded by a 1000 fps high-speed camera in this study. L_1 represents the maximum length of the outburst hole in the x direction (Fig. 15a); L_0 represents the width of the spallation area (Fig. 10); d represents the experimentally observed spallation thickness, where the thickness in the He tests is assumed to be 0.01 m; n_0 represents the number of spallation ejections obtained by L_1/d; $\overline{v_t}$ represents the mean propagation velocity of the outburst obtained by L_1/t; and $\overline{f_{sp}}$ represents the mean frequency of spallation ejections obtained by n_0/t.

With an increase in outburst pressure and adsorption capacity of the experimental gas, both $\overline{v_t}$ and $\overline{f_{sp}}$ exhibit increasing trends. In particular, when the outburst pressure increased, the amplitude was 0.38–8.76% for $\overline{v_t}$ and 1.28–12.07% for $\overline{f_{sp}}$, which also increased as gas adsorption increased. This further indicates that the gas desorption from coal can significantly increase the propagation velocity of the outburst, as well as the frequency of spallation ejections, which would enhance the destructiveness of the outburst.

Furthermore, as coal spallation is caused by tensile failure related to gas pressure differences (Eq. 1), which are characterized by an initial increase then a decrease (Fig. 11c), the instantaneous frequency of spallation ejections (f_{sp}) and the instantaneous propagation velocity of the outburst (v_t) may also exhibit a pattern of an initial increase followed by a decrease. In this case, when the gas pressure drops to approximately 2/3 of the outburst pressure, both v_t and f_{sp} reach their maxima, which may be the most destructive phase in the outburst process. Our experiments show that the final destructiveness of an outburst strongly depends on the peak values of these parameters mainly related to gas conditions. When extending this laboratory result to an actual underground mine, a set of possible magnitudes of an outburst can be predicted by estimating the values of specific parameters at the most destructive phase.

4.3 Effect of Gas Desorption on Outburst

Through experimental investigations, the contribution of gas desorption to the formation of coal spallation was determined. However, as it is difficult to estimate the amount of desorbed gas participating in an outburst, explaining the role of gas desorption from the perspective of kinetics is also difficult. Laboratory simulations provide a feasible way to show the contribution of desorbed gas from the perspective of energy conservation. Previous studies have concluded that, during an outburst, the gas expansion energy and the elastic energy of the coal are the main sources of the outburst energy that are consumed in the transport and crushing of coal, as well as the remaining kinetic energy of the gas (Jin et al. 2018; Tu et al. 2016; Zhao et al. 2016). In this case, the energy conservation equation can be expressed as follows:

$$E_0 + E_s = W_1 + W_2 + W_3, \tag{3}$$

where E_0 and E_s represent the elastic energy and the gas expansion energy (J), respectively; W_1 represents the energy consumption for outburst coal transport (J); W_2 represents the energy consumption for crushing the coal (J); and W_3 represents the residual kinetic energy (J).

For experiments without applied stress, when we assume that the elastic energy of the coal can be ignored and the gas expansion energy is completely consumed by the transport of the outburst coal (Jin et al. 2018; Tu et al. 2016; Zhao et al. 2017, 2016), Eq. (3) can be approximated by imposing $E_0 + E_s = W_1$ and $E_0 = 0$, in the following manner:

$$E_s = E_1 + E_2 = W_1, \tag{4}$$

where E_1 and E_2 represent the energy contributions of the desorbed gas and the free gas (J), respectively.

Contrastingly, the energy consumption for transporting the ejected coal (W_1) can be described by the formula for horizontal projectile motion (Fig. 16):

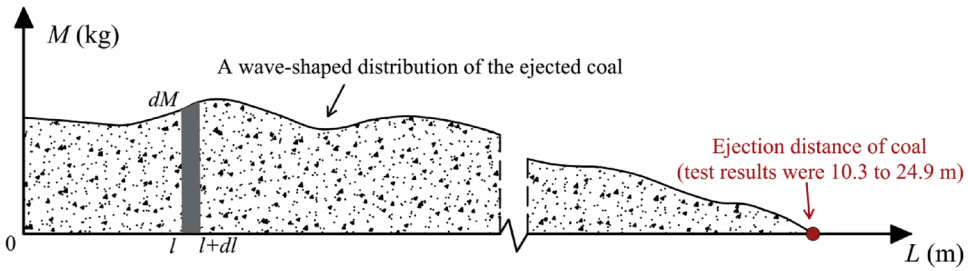

Fig. 16 Schematic diagram showing the deposition characteristics of the ejected coal. After each outburst experiment, the ejected coal was carefully collected at 1 m intervals and weighed

Table 5 Outburst energy at different conditions

Gas type	Outburst pressure (MPa)	E_1(J)	E_2(J)	W_1(J)	Contribution ratio (E_1/W_1, %)
He	0.5	–	632.75	632.75	–
He	0.6	–	997.78	997.78	–
He	0.7	–	1413.4	1413.4	–
N_2	0.5	551.83	632.75	1184.58	46.58
N_2	0.6	864.95	997.78	1862.73	46.43
N_2	0.7	1191.82	1413.4	2605.22	45.75
CO_2	0.5	2710.55	632.75	3343.30	81.07
CO_2	0.6	4287.63	997.78	5285.41	81.12
CO_2	0.7	6049.59	1413.4	7462.99	81.06

$$W_1 = \frac{1}{2} M_E {v_e}^2 = \frac{g \cdot M_E \cdot {L_E}^2}{4h} \tag{5}$$

$$L_E = \frac{1}{M_E} \sum_{i=1}^{n} (ldM), \tag{6}$$

where M_E is the intensity of outburst (kg); L_E is the equivalent distance of the coal ejection (m); g is the gravitational acceleration, g = 9.8 m/s^2; v_e is the speed of the ejected coal flow (m/s); and h is the characteristic height dimension of the ejected coal, $h = 0.6$m.

Based on the analyses of the energy principles [Eq. (3) to (6)], experimental results (Table 3), and depositional characteristic of the outburst coal, the outburst energy at different conditions was calculated (Table 5). The energy consumptions of the CO_2 and N_2 tests were considerably larger than those of the He tests (increase in amplitude ranges from 184.32 to 286.64%). In particular, the contribution of the desorbed gas is > 45.75% in the N_2 tests and > 81.06% in the CO_2 tests. This means that, with the participation of absorbed gas, the total outburst energy can be increased by 1.84–5.30 times, which would remarkably enhance the destructiveness of the outburst.

Furthermore, Fig. 17 shows the relationship between the contribution of desorbed gas (E_1) and the width of the spallation area (L_0). With an increase in E_1, L_0 exhibits a nearly linear growth trend ($R^2 = 0.99$), indicating that gas desorption is strongly associated with spallation formation, which further suggests that L_0 may be used as an index to compare the desorbed gas energy under similar environmental conditions. Although the estimation of the width of the spallation area is more difficult, compared with the indexes commonly used to measure the outburst destructiveness (outburst intensity, amount of gas released, and outburst distance), L_0 can better reflect the contribution of desorbed gas in the outburst development stage.

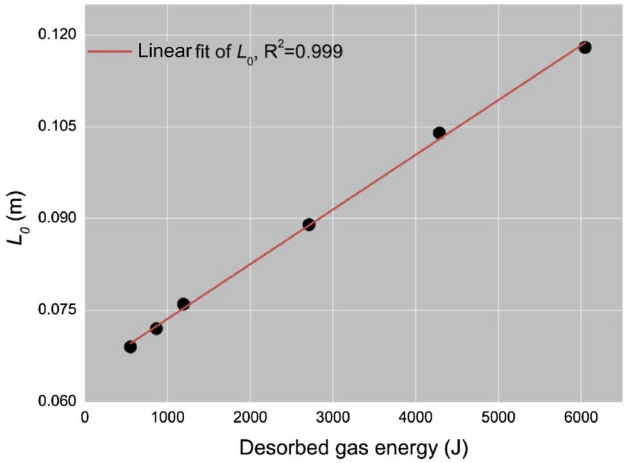

Fig. 17 Relationship between the desorbed gas energy and the width of the coal spallation area (L_0)

4.4 Comparison with Natural Outbursts

Due to technical limitations, certain significant outburst characteristics are difficult to obtain in underground mines, thereby limiting the investigation of outburst mechanisms. In this case, laboratory simulations can effectively replicate certain key outburst characteristics. Our experimental conditions differ from underground mines in two aspects. First, the porosity of our molded coal was approximately 19%, which is larger than typical values as observed in actual coal seams (An et al. 2013; Tu et al. 2016; Zhao et al. 2017). Second, the outburst coal in our experiments was ejected into an

open space rather than a roadway, which may have altered the transportation process of the coal–gas flow.

As low porosities result in low permeabilities (Cheng and Pan 2020; Pan and Connell 2007, 2012), the permeability of the molded coal in this study is inevitably greater than the permeability of primary coal. Thus, for a real outburst disaster, a pressure gradient will be developed and maintained more easily than in this study. Therefore, in situ circumstances will be more susceptible to the development of a spallation area. Moreover, when we assume that the porosity of the coal sample was 6%, then the free gas energy is only 30% of that shown in Table 5. In this case, due to the effect of gas desorption, the energy contribution of the desorbed gas accounts for 73.8–93.5%, and the total outburst energy accordingly increases by 3.89–15.32 times. This further indicates that the formation of coal spallation, as well as the destructive potential of outbursts, depends on the energy contribution from the desorbed gas.

Under natural conditions, due to the position of the outburst hole and dips in the roadways, it is difficult to maintain horizontal ejection during an outburst (Jin et al. 2011). Nevertheless, certain outbursts, particularly in roadways with small dips, will produce wave-shaped distributions of outburst coal. The Xinxing outburst, a disaster that occurred in the Xinxing coal mines of China on November 21, 2009, was a typical case. As shown in Fig. 18, we can observe a fluctuation of the height along the roadway, although this fluctuation is not evident. In an actual scenario, numerous large coal pieces or rock lumps would be accumulated in the roadway (especially in the space near the outburst hole) with coal powder, which is a more probable cause than gas–solid flow. Thus, for simulation experiments where coal powders are easier to form, the wave-shaped distribution is more apparent.

5 Conclusions

One of the major goals of experimental research on outbursts is to develop models that can link hazard characteristics to specific physical factors. In this study, some distinct properties of the coal spallation area were revealed for the first time, such as its emergence conditions and formation characteristics. In particular, we have provided a viable mechanism to explain the development of a coal spallation area, which is critical in understanding the outburst propagation. More importantly, we have associated different outburst characteristics with different expressions of outburst factors. According to our findings, the following conclusions can be drawn:

1. Outbursts can occur as long as the gas pressure reaches a certain threshold, regardless of the stress conditions. In the outburst development stage, coal spallation represents a common failure type, and its formation shows periodicity typically leading to a wave-shaped distribution of the ejected coal. However, the formation of a spallation area is not an inevitable result which depends on whether a sufficient internal pressure gradient can be formed near the exposed surface. Instead, the development of a spallation area is related to multiple physical factors including gas pressure, coal permeability, and stress, where gas ad-/desorption plays a decisive role. When extending these laboratory results to real outburst disasters (where the permeability of the coal seam is

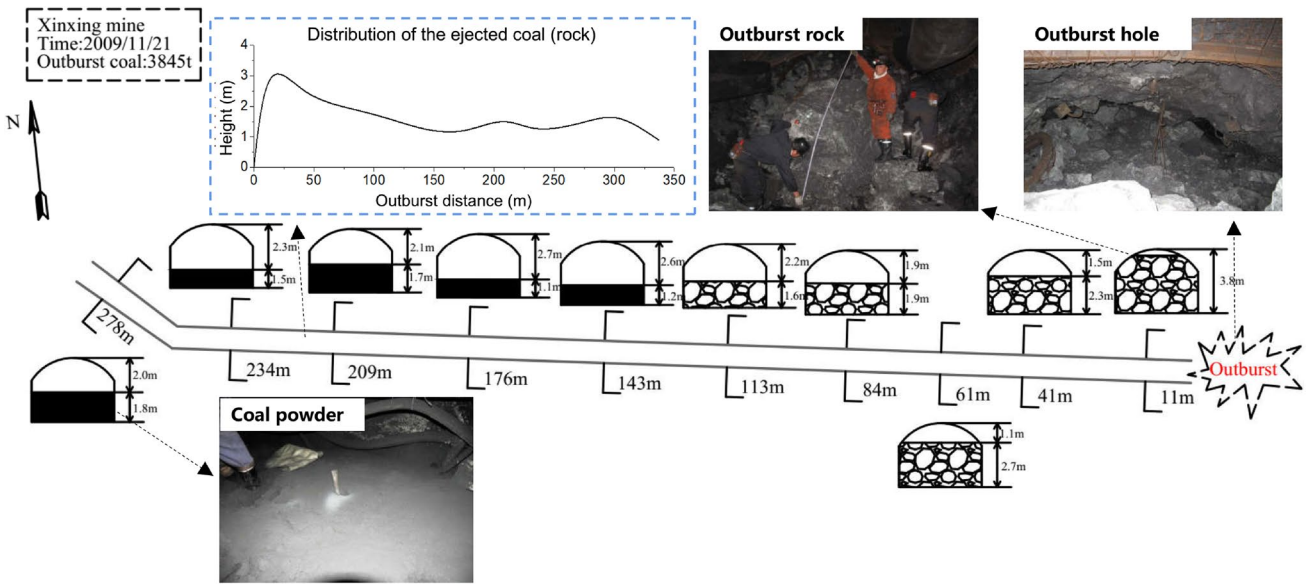

Fig. 18 Distribution of ejected coal in the 2009 Xinxing outburst

smaller), the natural circumstances will be more susceptible to the development of a spallation area. Hence, our results necessitate collecting this unique characteristic in natural outbursts, as it has significant value in analyzing the development of outbursts, although being rarely captured.

2. Gas desorbed from coal has a significant influence on the outburst coal–gas flow, resulting in a longer ejection distance and a stronger ejected coal conveying capacity. Its contribution ratio could reach 45.75–81.12%, which would increase the gas expansion energy by 1.84–5.30 times. Moreover, with an increase in the desorbed gas energy, the width of the spallation area (L_0) exhibited a nearly linear growth trend. Our results further indicate that, in addition to the destructiveness of outbursts, L_0 also is affected by gas desorption. When applying these experimental results to an actual mine (where the porosity of the coal seam is assumed to be 6%), first, the dominance of gas desorption is more significant, which could increase the total outburst energy by 3.89–15.32 times; second, L_0 may be developed as a new index to measure and compare the magnitude of the outburst energy in underground conditions.
3. With an increase in outburst pressure and adsorption capacity of the experimental gas, both the mean propagation velocity of the outburst and mean frequency of the spallation ejections exhibited an increasing trend, which would enhance the destructiveness of the outburst. More importantly, when the gas pressure drops to approximately 2/3 of the outburst pressure, their instantaneous values may reach their maxima, which controls the outburst destructiveness to some extent. This indicates that by estimating the peak of certain parameters, a set of possible magnitudes of an outburst can be well predicted.
4. Our results highlight that understanding the mechanism of spallation area formation is crucial for accurately interpreting the outburst development. In future research, we will focus on (a) employing solid mechanics for further quantitative analysis; (b) extending our analysis to high stress conditions; and (c) revealing the dynamics of outburst through other key features, including high-speed coal–gas flow, rapid desorption of gas, and pulverized coal.

Acknowledgements We thank the editor and two anonymous reviewers for insightful comments, criticisms, and suggestions. This research was supported by the National Natural Science Foundation of China (No. 51874294, 52034008), and the Priority Academic Program Development of Jiangsu Higher Education Institutions (PAPD).

Declarations

Conflict of interest The authors declare that we do not have any commercial or associative interest that represents a conflict of interest in connection with the work submitted.

References

Aguado MBD, Nicieza CG (2007) Control and prevention of gas outbursts in coal mines, Riosa-Olloniego coalfield, Spain. Int J Coal Geol 69:253–266

An F, Cheng Y, Wang L, Li W (2013) A numerical model for outburst including the effect of adsorbed gas on coal deformation and mechanical properties. Comput Geotech 54:222–231

Beamish BB, Crosdale PJ (1998) Instantaneous outbursts in underground coal mines: an overview and association with coal type. Int J Coal Geol 35:27–55

Bodziony J, Lama R (1996) Sudden outbursts of gas and coal in underground coal mines. ACARP, Australia

Busch A, Gensterblum Y, Krooss BM, Siemons N (2006) Investigation of high-pressure selective adsorption/desorption behaviour of CO 2 and CH 4 on coals: an experimental study. Int J Coal Geol 66:53–68

Cao Y, He D, Glick DC (2001) Coal and gas outbursts in footwalls of reverse faults. Int J Coal Geol 48:47–63

Cheng Y, Pan Z (2020) Reservoir properties of Chinese tectonic coal: A review. Fuel 260:116350

Cui Y, Zhang Q (2005) Adsorption of different rank coals to single component gases. J Nat Gas Ind 25:61–68

Durucan S, Edwards J (1986) The effects of stress and fracturing on permeability of coal. Min Sci Technol 3:205–216

Fan C, Li S, Luo M, Du W, Yang Z (2017) Coal and gas outburst dynamic system. Int J Min Sci Technol 27:49–55

Guan P, Wang H, Zhang Y (2009) Mechanism of instantaneous Coal Outbursts. Geology 37:915–918

Guo P (2014) Research on laminar spallation mechanism of coal and gas outburst propagation. China University of Mining and Technology, China

Hu QT, Zhou SN, Zhou XQ (2008) Mechanical mechanism of coal and gas outburst process. J China Coal Soc 33:1368–1372

Hu B et al (2020) New insights into the CH4 adsorption capacity of coal based on microscopic pore properties. Fuel. https://doi.org/10.1016/j.fuel.2019.116675

Jasinge D, Ranjith P, Choi S (2011) Effects of effective stress changes on permeability of latrobe valley brown coal. Fuel 90:1292–1300

Jiang C, Yu Q (1995) Spherical shell destabilization hypothesis on coal and gas outburst mechanism. Saf Coal Mines 2:17–25

Jin H, Hu Q, Liu Y (2011) Failure mechanism of coal and gas outburst initiation. Proc Eng 26:1352–1360

Jin K et al (2018) Experimental investigation on the formation and transport mechanism of outburst coal-gas flow: implications for the role of gas desorption in the development stage of outburst. Int J Coal Geol 194:45

Khristianovich S (1953) Distribution of gas pressure close to an advancing coal face. Irv Anussr Otd Tekhn Nauk 12:1673–1678

Kursunoglu N, Onder M (2019) Application of structural equation modeling to evaluate coal and gas outbursts. Tunn Undergr Space Technol 88:63–72

Lama RD, Bodziony J (1998) Management of outburst in underground coal mines. Int J Coal Geol 35:83–115

Lei Y, Cheng Y, Ren T, Tu Q, Shu L, Li Y (2021) The energy principle of coal and gas outbursts: experimentally evaluating the role of gas desorption. Rock Mech Rock Eng 55:11–30

Li XC, Nie BS, He XQ, Zhang X, Yang T (2011) Influence of gas adsorption on coal body. J China Coal Soc 36:2035

Lin J, Ren T, Wang G, Booth P, Nemcik J (2018) Experimental investigation of N2 injection to enhance gas drainage in CO2-rich low permeable seam. Fuel 215:665–674

Litwiniszyn J (1983) A model of rock and gas mass outburst. Arch Min Sci 28:453–466

Long QM, Zhao XS, Shun DL, Zhou YH (2008) Experimental study on coal permeability by adsorption. J China Coal Soc 33:72–76

Mcgarr A (1997) A mechanism for high wall-rock velocities in rockbursts. Birkhäuser Basel, Basel

Medhurst T, Brown E (1998) A study of the mechanical behaviour of coal for pillar design. Int J Rock Mech Min Sci 35:1087–1105

Pan Z, Connell LD (2007) A theoretical model for gas adsorption-induced coal swelling. Int J Coal Geol 69:243–252

Pan Z, Connell LD (2012) Modelling permeability for coal reservoirs: a review of analytical models and testing data. Int J Coal Geol 92:1–44

Sakurovs R, Day S, Weir S (2012) Relationships between the sorption behaviour of methane, carbon dioxide, nitrogen and ethane on coals. Fuel 97:725–729

Skoczylas N, Ijrmms J (2012) Laboratory study of the phenomenon of methane and coal outburst. Int J Rock Mech Min Sci 55:102–107

Skoczylas N, Dutka B, Sobczyk J (2014) Mechanical and gaseous properties of coal briquettes in terms of outburst risk. Fuel 134:45–52

Tu Q, Cheng Y, Guo P, Jiang J, Wang L, Zhang R (2016) Experimental study of coal and gas outbursts related to gas-enriched areas. Rock Mech Rock Eng 49:1–13

Tu Q, Cheng Y, Liu Q, Guo P, Wang L, Li W, Jiang J (2018) Investigation of the formation mechanism of coal spallation through the cross-coupling relations of multiple physical processes. Int J Rock Mech Min Sci 105:133–144

Vardoulakis I (1984) Rock bursting as a surface instability phenomenon. Int J Rock Mech Min Sci Geomech Abstr 21:137–144

Wang C, Yang S, Yang D, Li X, Jiang C (2018) Experimental analysis of the intensity and evolution of coal and gas outbursts. Fuel 226:252–262

Yang W et al (2018) Outburst mechanism of tunnelling through coal seams and the safety strategy by using "strong-weak" coupling circle-layers. Tunn Undergr Space Technol 74:107–118

Zhang Y, Kling GW (2006) Dynamics of lake eruptions and possible ocean eruptions. Annu Rev Earth Planet Sci 34:293–324

Zhao W, Cheng Y, Jiang H, Jin K, Wang H, Wang L (2016) Role of the rapid gas desorption of coal powders in the development stage of outbursts. J Nat Gas Sci Eng 28:491–501

Zhao W, Cheng Y, Guo P, Jin K, Tu Q, Wang H (2017) An analysis of the gas-solid plug flow formation: new insights into the coal failure process during coal and gas outbursts. Powder Technol 305:39–47